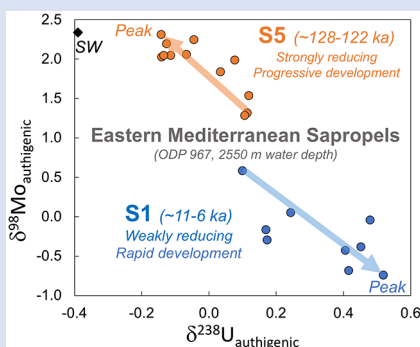# Rapid onset of ocean anoxia shown by high U and low Mo isotope compositions of sapropel S1

M.B. Andersen[1,2,3*], A. Matthews[4], M. Bar-Matthews[5], D. Vance[2]

OPEN ACCESS

Abstract

Authigenic uranium isotope compositions of Holocene sapropel S1 ($\delta^{238}U_{auth}$ = + 0.10 to +0.52 ‰; ODP core 967, 2550 mbsl) are significantly higher than the proposed upper boundary (+0.2 ‰) associated with the transport-porewater diffusion model for sediment uranium uptake. It is shown that these high $\delta^{238}U_{auth}$ values are compatible with rapid initial slowdown of thermohaline overturning and the development of an anoxic water column. These conditions would favour U uptake in an organic-rich floccule layer overlying the sediment-water interface. The high $\delta^{238}U_{auth}$ values correlate with low $\delta^{98}Mo_{auth}$ values (+0.02 to −0.88 ‰), interpreted to reflect weakly euxinic conditions controlled by thiomolybdate–molybdate solution equilibria. The S1 data contrast markedly with published data from last interglacial sapropel S5 from the same core, which show $\delta^{238}U_{auth}$ and $\delta^{98}Mo_{auth}$ characteristics compatible with a restricted euxinic basin due to progressive slowdown in the thermohaline circulation. The U-Mo isotope data for S1 are similar to a range of published palaeo-settings. Sapropels are therefore shown to be useful templates for the unravelling of the interplay between productivity and deep water renewal times in ancient settings.

Introduction

The redox sensitive behaviour and associated isotope fractionations of molybdenum (Mo) and uranium (U) have led to a prominent role for their sedimentary and isotope geochemistry in the evaluation of ancient ocean redox conditions. Both elements can show strong authigenic (seawater-derived) enrichment in marine organic carbon-rich sediments, accompanied by distinctive isotope signatures (e.g., Asael et al., 2013; Kendall et al., 2015; Brüske et al., 2020).

Uranium isotopes in anoxic and organic carbon-rich marine sediments (expressed as $\delta^{238}U$, parts per thousand deviation from the CRM145 standard) generally show values considerably heavier than contemporary seawater (−0.39 ‰; Andersen et al., 2017). This isotope enrichment is compatible with partial reduction of U^{+6} to U^{+4}. In modern organic carbon-rich sediments, authigenic $\delta^{238}U$ values rarely exceed +0.2 ‰, equivalent to a $\Delta^{238}U_{sediment-water}$ of ~ +0.6 ‰, approximately half the estimated full isotope fractionation accompanying U reduction (Andersen et al., 2017). This has been interpreted in terms of a diffusion-reaction-transport model combining U reduction in the semi-closed sediment system, limited by U diffusion from bottom water through pore waters (Andersen et al., 2014). However, an increasing number of ancient organic carbon-rich sediments show authigenic $\delta^{238}U$ values higher than +0.2 ‰, suggesting redox-driven U isotope fractionation closer to that expected in an open system ($\Delta^{238}U$ > +0.6 ‰), and pointing towards U reduction outside the sediments (e.g., Brüske et al., 2020; Cheng et al., 2020; Kendall et al., 2020).

In addition, coupled measurements of molybdenum isotope compositions (expressed as $^{98}Mo/^{95}Mo$, parts per thousand deviation from NIST 3134 at +0.25; Nägler et al., 2014) in these high $\delta^{238}U$ organic carbon-rich sediments, generally show $\delta^{98}Mo$ significantly lower than the modern seawater value of ~ +2.3 ‰ (e.g., Cheng et al., 2020; Kendall et al., 2020). Near seawater $\delta^{98}Mo$ values are proposed to reflect euxinic water conditions, where dissolved $[H_2S]_{aq}$ exceeds a 'switch point' (~11 μM for modern seawater) at which seawater MoO_4^{2-} becomes irreversibly and near-quantitatively converted to a highly particle reactive tetra-thiomolybdate (MoS_4^{2-}) species (Erickson and Helz, 2000; Arnold et al., 2004). Euxinic waters with $[H_2S]_{aq}$ below the switch point, may lead to Mo deposition with significantly lower $\delta^{98}Mo$ values because Mo removal occurs from isotopically fractionated oxy-thiomolybdate species coexisting with molybdate (Neubert et al., 2008; Kerl et al., 2017). An alternative mechanism for the generation of isotopically light Mo relates to the delivery of authigenic Mo to sediments via a Fe-Mn oxide particulate shuttle (Kendall et al., 2017).

1. Cardiff University, School of Earth & Ocean Sciences, Park Place, Cardiff CF10 3AT, United Kingdom
2. ETH Zürich, Institute of Geochemistry and Petrology, Department of Earth Sciences, Clausiusstrasse 25, 8092 Zurich, Switzerland
3. Bristol Isotope Group, School of Earth Sciences, University of Bristol, Wills Memorial Building, Queen's Rd, Bristol BS8 1RJ United Kingdom
4. Institute of Earth Sciences, Hebrew University of Jerusalem, 9190401 Jerusalem, Israel
5. Geological Survey of Israel, 32 Yesha'ayahu Leibowitz St., 9692100 Jerusalem, Israel

* Corresponding author (email: andersenm1@cardiff.ac.uk)

Though this combination of high $\delta^{238}U$ and low $\delta^{98}Mo$ is observed in a range of ancient sediments, an understanding of the specific biogeochemical and oceanographic settings that cause it is hindered by the lack of well-studied modern analogues. The periodic deposition of organic carbon-rich sediments (sapropels) in the Eastern Mediterranean (EM) sea provide a means to study the behaviour of this coupled redox proxy system. In particular, the study of sapropels of different intensity at different times in the same physical setting allows the identification of signatures driven by different climatic and oceanographic forcing mechanisms.

Authigenic U and Mo Isotopes in Sapropels S1 and S5

This study investigates the contrasting U and Mo isotope systematics of EM sapropels S1 from the Holocene and S5 from the last interglacial (abbreviated 'S1' and 'S5' in the following), sampled in ODP core 967 (SI; Fig. S-1). Sapropel S5 (~128.3–121.5 ka) shows strong authigenic enrichment of U and Mo, coupled to progressive $\delta^{98}Mo_{auth}$ increase (+1.2 to +2.3 ‰) and $\delta^{238}U_{auth}$ decrease (+0.10 to −0.15 ‰), from the beginning to the end (Andersen *et al.*, 2018). Modelling of the S5 $\delta^{238}U$ indicates a progressive 10 fold decline in the deep EM thermohaline overturning circulation. A study of S1 (10.8–6.1 ka) has shown that it is less strongly developed than S5, with weakly sulfidic bottom water conditions interpreted from low $\delta^{98}Mo$ values (Azrieli-Tal *et al.*, 2014), although anoxic conditions were regionally prevalent at water depths >1800 m (de Lange *et al.*, 2008).

Here, we report additional U isotope measurements for S1, allowing a direct comparison of the U and Mo isotope systematics for S1 and S5 (methods, age models and additional data are summarised in SI). The S1 samples show lower U concentrations (10–40 ppm) than S5 (25–150 ppm), but high $\delta^{238}U$ values, reaching +0.35 to +0.5 ‰ in the lower and middle zones at 127–116 cm (Fig. 1). Thus, both the U concentration and $\delta^{238}U$ patterns in S1 differ significantly from S5. Calculated authigenic U (U_{auth}) and Mo (Mo_{auth}) concentrations in the S1 profile show that detrital contributions are only significant in the background sediments, whereas authigenic contributions dominate in S1 (85–96 %). High U_{auth} concentrations are correlated with high $\delta^{238}U_{auth}$ values (> +0.2 ‰) and high Mo_{auth} concentrations with low $\delta^{98}Mo$ values (Fig. 1). Peak $\delta^{238}U_{auth}$ values (127–116 cm) vary from +0.41 ± 0.06 ‰ to +0.52 ± 0.06 ‰, whereas $\delta^{238}U_{auth}$ values of −0.7 to +0.1 ‰ occur before and after S1 and in the first sample at its start (130 cm), indicating that a significant proportion of the U_{auth} may be associated with U deposited directly with organic matter, carrying low $\delta^{238}U_{auth}$ (Andersen *et al.*, 2017), in addition to *in situ* U reduction (see SI for details).

Controls on U and Mo Isotope Fractionation in S1 and S5

Sapropels S1 and S5 show contrasting behaviour in their $\delta^{238}U$-$\delta^{98}Mo$ systematics, which may relate to different climatic and oceanographic mechanisms creating sediment and/or seawater anoxia. Firstly, the timing of peak sapropel development, as expressed in redox sensitive trace metal profiles, represents a
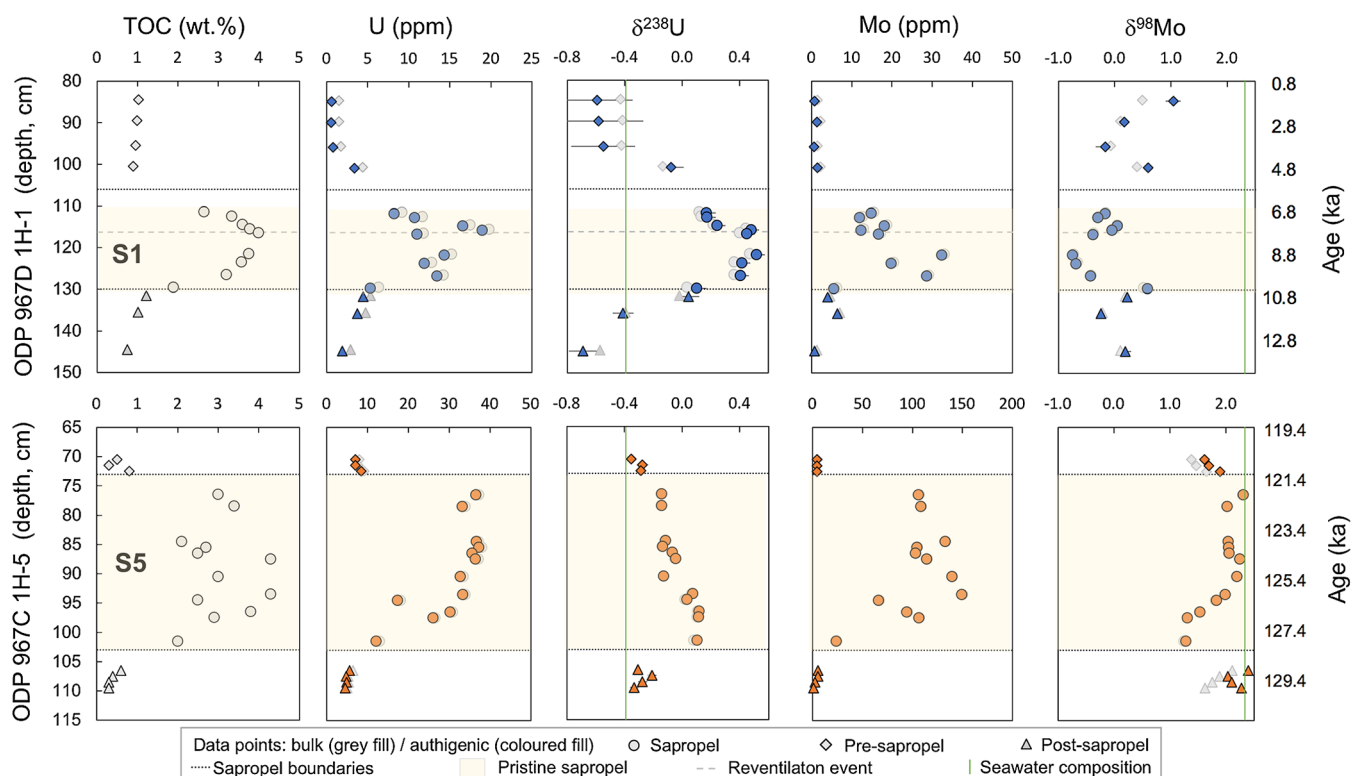
Figure 1 Depth profiles for sapropels S1 (top) and S5 (bottom). The S5 data are from Andersen *et al.* (2018), the S1 Mo data from Azrieli-Tal *et al.* (2014). Dashed lines indicate the position of the sapropel boundaries as determined from Ba/Al ratios. The TOC profile in S1 indicates post-sapropel oxidation in the upper 4 cm (see SI). A potential post-deposition ventilation event at ~116 cm (8 ka) is marked with weakly stippled line for S1. Vertical lines in the isotope panels represent approximate seawater compositions. Note the larger scale bars for S5 than S1 for the U (x2) and Mo (x4) concentrations.

key difference between the two sapropels. Whereas redox sulfide sensitive proxies for S1 (S, Fe/Al, V/Al, Mo/Al, As/Al) indicate rapid and early development to maximum intensity at *ca.* 120 cm, the same proxies show that S5 developed more slowly, only reaching maximum values in the upper sapropel (SI; Fig. S-2). The higher concentrations of redox sensitive trace metals (*e.g.*, U and Mo concentration profiles; Fig. 1) also demonstrate the more reducing character of S5. In contrast, the two sapropels do not show any systematic differences in TOC at peak sapropel conditions (Fig. 1), and they have similar calculated organic carbon accumulation rates (OCAR) of 261 ± 36 mg/cm^2·kyr for S1 and 178 ± 48 mg/cm^2·kyr for S5 (see SI for details).

The $\delta^{98}Mo_{auth}$ of S1 shows a significant early drop towards the low values of ~ -0.8 ‰ at peak sapropel conditions, followed by a rise to ~ 0 ‰ (Fig. 1). The low S1 $\delta^{98}Mo$ values have been interpreted to represent Mo uptake from isotopically fractionated oxy-thiomolybdate species at bottom water sulfide levels below that at which Mo is effectively and near-quantitatively converted to tetra-thiomolybdate (Azrieli-Tal *et al.*, 2014). The production of thiomolybdates requires sulfate reduction, driven by biological productivity and long deep water replacement times. Non-quantitative conversion of Mo to thiomolybdate requires low sulfide and sequestration of more sulfidised species to the sediment, *e.g.*, by colloidal FeMo(VI)S$_4$ (Helz and Vorlicek, 2019). Low sulfide levels and non-quantitative conversion of molybdate to thiomolybdates can result in isotopically light sedimentary Mo without invoking a Fe-Mn shuttle, *via* non-quantitative Mo removal from bottom waters, in a similar way as suggested for a range of modern semi-closed basins also showing authigenic $\delta^{98}Mo$ values below seawater (Bura-Nakic *et al.*, 2018). In S5, with more intense sulfate reduction resulting from protracted thermohaline overturning slowdown and high OCAR, the $\delta^{98}Mo_{auth}$ are close to the seawater values (Andersen *et al.*, 2018).

In contrast to S5, S1 is characterised by high $\delta^{238}U$, higher than expected from reduction of seawater-derived U in a semi-closed sediment-porewater system (Andersen *et al.*, 2014). Post-sapropel oxidative burndown leading to diagenetic redistribution of previously deposited, isotopically fractionated U downwards, could provide a mechanism for creating high $\delta^{238}U$. However, the expression of the oxidative burndown in S1 is distinct and sharp for all the redox sensitive metals. There is no evidence for downwards U diffusion and reprecipitation (*e.g.*, a gradient in U/Al and $\delta^{238}U$ with depth – see SI for details). Alternatively, U isotope reactive-transport modelling has suggested that high $\delta^{238}U$ could be a consequence of low sedimentation rates and high productivity in reducing sediments (Lau *et al.*, 2020). However, the similar sedimentation rates for S1 and S5, also make this an unlikely process given their very different $\delta^{238}U$ signatures (Fig. 1). Direct U reduction in the water column, followed by scavenging and transport to the sediments, is another mechanism that could lead to high $\delta^{238}U$ (*e.g.*, Brüske *et al.*, 2020; Kendall *et al.*, 2020). But the stronger uptake of redox sensitive metals in S5 than S1 (Fig. 1) would likely favour high $\delta^{238}U$ in S5, not S1.

Another model for providing a greater expression of the $\Delta^{238}U_{sediment-water}$ involves U reduction promoted by an organic-rich floccule layer overlying the consolidated sediment (Andersen *et al.*, 2017; Cheng *et al.*, 2020). The formation of an organic-rich floccule layer is likely to occur in settings with high biological productivity and organic carbon flux. However, the combined Mo-U data for S1 require a further condition: light Mo isotopes require the partial conversion of Mo to thiomolybdate, and therefore mildly sulfidic levels. Redox sensitive element data for S1 (Figs. 1, S-2) make a strong case for rapid early development of euxinia, which could promote deposition of such an

organic-rich floccule layer. High resolution simulations of intermediate and deep water circulation suggest that enhanced Nile discharge could have triggered rapid shutdown of EM overturning circulation (Vadsaria *et al.*, 2019). The early thermohaline circulation slowdown would potentially promote the development of mildly sulfidic waters.

Outlook: the U-Mo Isotope Proxy Applied to Ancient Sediments

Both S1 and S5 show inverse correlations between $\delta^{238}U_{auth}$ and $\delta^{98}Mo_{auth}$ (Fig. 2). However, temporally, the trends go in opposite directions. For S5, the end point of the correlation is defined by maximal euxinic conditions at the end of the sapropel. In S1, the end point of the correlation is represented by the early sapropel peak. This difference in temporal progression for S1 and S5 is likely to reflect the fundamentally different modes of Mo and U incorporation into the sediments. Whilst the S5 data likely records progressive slowdown and increasingly euxinic conditions throughout the entirety of sapropel formation (Andersen *et al.*, 2018), S1 seems to require rapid short-lived euxinia caused by early thermohaline slowdown. These two scenarios provide a potential framework for the interpretation of palaeo-redox evolution. Using the sapropel data, it is possible to delineate three general behaviours (Fig. 2). The first (1) represents mildly euxinic sediments typical of S1, with U and Mo uptake associated with an organic floccule layer. The second (2) is associated with non-quantitative U and Mo uptake in more intensely euxinic conditions and with porewater U reduction. The third (3) involves strongly euxinic sediments moving towards near-quantitative Mo and U uptake, as seen in S5 and in modern restricted basins with variable deep water overturning rates (Fig. 2).

Trend (1), seen in S1, is very similar to recent published combined $\delta^{238}U_{auth}$ - $\delta^{98}Mo_{auth}$ data from Cambrian and Devonian organic carbon-rich sediments (Cheng *et al.*, 2020; Kendall *et al.*, 2020). These sediments show high $\delta^{238}U$ values (up to $+0.6$ ‰), combined with low $\delta^{98}Mo$ (down to -0.1 ‰). Also, Ediacaran organic–rich mudstones (Kendall *et al.*, 2015) and the Palaeoproterozoic Zaonega Formation shales (Asael *et al.*, 2013) show an inverse correlation which parallels the type 1 (S1) trend. Limited Black Sea unit II data (Brüske *et al.*, 2020) show similarly high $\delta^{238}U_{auth}$ ($\sim +0.55$ ‰) to S1, while $\delta^{98}Mo_{auth}$ ($+1.23$ ‰) is relatively high (Fig. 2). All these localities exhibit similar negatively correlated $\delta^{238}U$- $\delta^{98}Mo$ values as seen in S1, but at variable trajectories and with different $\delta^{98}Mo$ values. This observation may be partly attributed to variable seawater $\delta^{98}Mo$ over time, but it would also depend on the [H$_2$S]$_{aq}$ levels and the specific stability of the oxy-thiomolybdate species in each setting.

A key observation is that although high productivity in upwelling-type settings has been suggested to be the critical driver for high $\delta^{238}U$ in organic carbon-rich sediments (Cheng *et al.*, 2020), this does not fit well with the observations in this study. Although high productivity is an important factor it is not the defining one (*e.g.*, S1 and S5 have similar TOC contents and calculated OCAR, yet show completely contrasting behaviour in the U and Mo isotope systematics). From the sapropel data it may be inferred that the specific conditions that favour combined high $\delta^{238}U_{auth}$ with low $\delta^{98}Mo_{auth}$ require both a high particulate to water ratio (*e.g.*, the organic floccule layer) and (low) [H$_2$S]$_{aq}$ levels, to aid the reduction of U and formation of oxy-thiomolybdates, followed by Mo and U scavenging by particulate/organic matter to the sediments. In the case of S1 this likely occurs *via* rapid thermohaline slowdown combined with
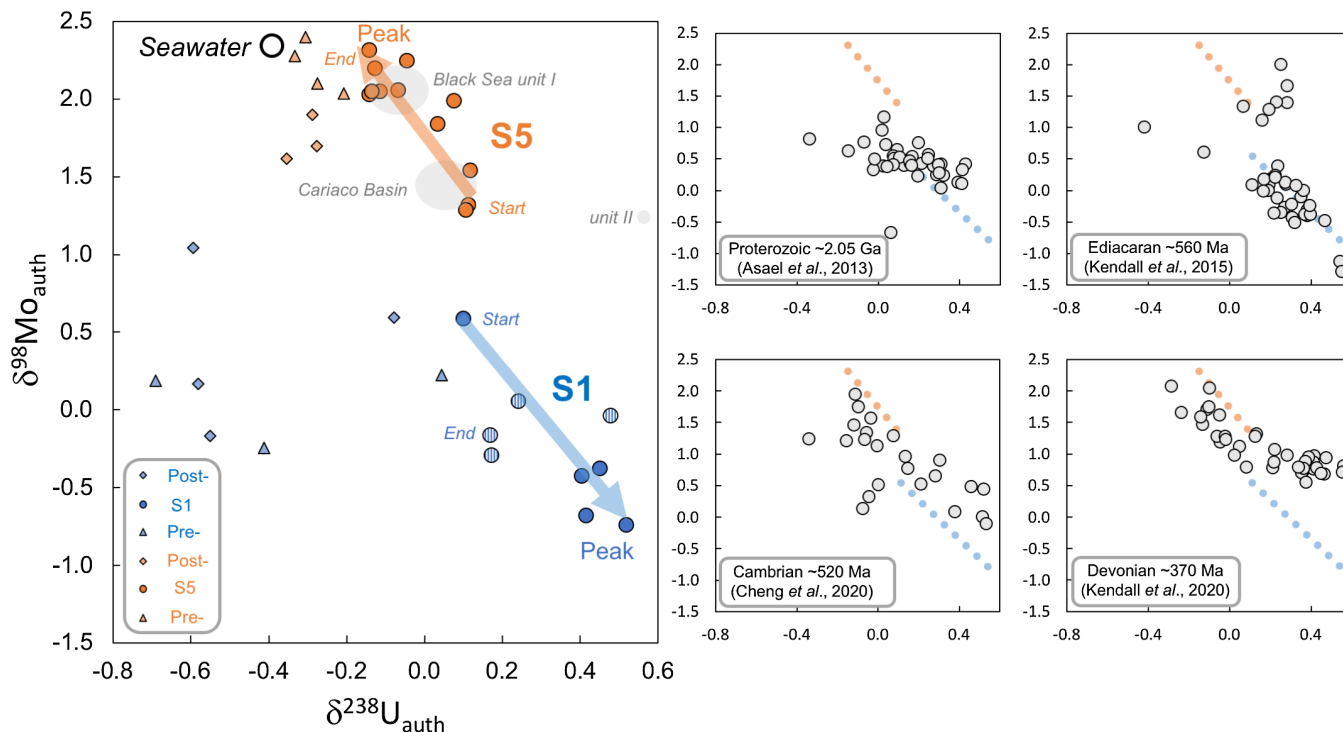
Figure 2 $\delta^{98}Mo_{auth}$ *vs.* $\delta^{238}U_{auth}$ crossplots for sapropels (main plot), as well as four Proterozoic to Devonian organic-rich shales (Asael *et al.*, 2013; Kendall *et al.*, 2015; Cheng *et al.*, 2020; Kendall *et al.*, 2020). The main plot shows S1 (blue, filled samples 130–116 cm, stippled 116–110 cm), sapropel S5 (orange) and background sediments. Compositions for modern day seawater and average deep sediments in Cariaco Basin and Black Sea Unit I/II (cores 12GGC/70GGC and 32MUC24, respectively; Brüske *et al.*, 2020) are also shown. Correlated linear relations for the sapropels from start towards peak sapropel maxima are shown by the arrows for S1 and S5. The four palaeo-data sets (converted to authigenic compositions – see SI), identify high $\delta^{238}U$ values combined with low $\delta^{98}Mo$, and generally similar evolutions to the S1 trend in the main plot (S5 and S1 trends marked by stippled lines).

high productivity and formation of an organic floccule layer. In other settings with high productivity in upwelling zones, the development of $[H_2S]_{aq}$ bottom water plumes as observed on the Peru margin (Schunck *et al.*, 2013), combined with an organic floccule layer, could also provide the right condition for high $\delta^{238}U_{auth}$ with low $\delta^{98}Mo_{auth}$ in organic carbon-rich sediments. The palaeo-examples discussed here show that conditions that favour these S1 type $\delta^{238}U$- $\delta^{98}Mo$ sediment systematics likely occurred across a large part of Earth history. Yet, in inferring palaeo-proxy evolution from U and Mo isotope trends, it is the data systematics from individual settings that are important, as opposed to direct comparison of exact $\delta^{238}U$ and $\delta^{98}Mo$ compositions between settings. Based on this study, the careful and combined analysis of $\delta^{238}U$- $\delta^{98}Mo$ systematics in organic carbon-rich sediments is critical to providing the most robust way of identifying localised isotope effects for both systems and, thus, oceanographic conditions during sediment deposition.

Acknowledgements

Additional Information

Cite this letter as: Andersen, M.B., Matthews, A., Bar-Matthews, M., Vance, D. (2020) Rapid onset of ocean anoxia shown by high U and low Mo isotope compositions of sapropel S1. *Geochem. Persp. Let.* 15, 10–14.

References

ANDERSEN, M.B. ROMANIELLO, S., VANCE, D., LITTLE, S.H., HERDMAN, R., LYONS, T.W. (2014) A modern framework for the interpretation of 238U/235U in studies of ancient ocean redox. *Earth and Planetary Science Letters* 400, 184–194.

ANDERSEN, M.B., STIRLING, C.H., WEYER, S. (2017) Uranium isotope fractionation. *Reviews in Mineralogy and Geochemistry* 82, 799–850.

ANDERSEN, M.B., MATTHEWS, A., VANCE, D., BAR-MATTHEWS, M., ARCHER, C., DE SOUZA, G.F. (2018) A 10-fold decline in the deep Eastern Mediterranean thermohaline overturning circulation during the last interglacial period. *Earth and Planetary Science Letters* 503, 58–67.

ARNOLD, G.L., ANBAR, A.D., BARLING, J., LYONS, T. (2004) Molybdenum isotope evidence for widespread anoxia in Mid-Proterozoic oceans. *Science* 304, 87–90.

ASAEL, D., TISSOT, F.L., REINHARD, C.T., ROUXEL, O., DAUPHAS, N., LYONS, T.W., PONZEVERA, E., LIORZOU, C., CHÉRON, S. (2013) Coupled molybdenum, iron and uranium stable isotopes as oceanic paleoredox proxies during the Paleoproterozoic Shunga Event. *Chemical Geology* 362, 193–210.

AZRIELI-TAL, I., MATTHEWS, A., BAR-MATTHEWS, M., ALMOGI-LABIN, A., VANCE, D., ARCHER, C., TEUTSCH, N. (2014) Evidence from molybdenum and iron isotopes and molybdenum–uranium covariation for sulphidic bottom waters during Eastern Mediterranean sapropel S1 formation. *Earth and Planetary Science Letters* 393, 231–242.

BRÜSKE, A., WEYER, S., ZHAO, M.-Y., PLANAVSKY, N.J., WEGWERTH, A., NEUBERT, N., DELLWIG, O., LAU, K.V., LYONS, T.W. (2020) Correlated molybdenum and uranium isotope signatures in modern anoxic sediments: implications for their use as paleo-redox proxy. *Geochimica et Cosmochimica Acta* 270, 449–474.

BURA-NAKIĆ, E., ANDERSEN, M.B., ARCHER, D., de SOUZA, G.F., MARGUŠ, M., VANCE, D. (2018) Coupled Mo-U abundances and isotopes in a small marine euxinic basin: Constraints on processes in euxinic basins. *Geochimica et Cosmochimica Acta* 222, 212–222.

CHENG, M., LI, C., JIN, C., WANG, H., ALGEO, T.J., LYONS, T.W., ZHANG, F. and ANBAR, A. (2020) Evidence for high organic carbon export to the early Cambrian seafloor. *Geochimica et Cosmochimica Acta,* doi: 10.1016/j.gca.2020.01.050.

de LANGE, G.J., THOMSON, J., REITZ, A., SLOMP, C.P., SPERANZA PRINCIPATO, M., ERBA, E., CORSELLI, C. (2008) Synchronous basin-wide formation and redox-controlled preservation of a Mediterranean sapropel. *Nature Geoscience* 1, 606–610.

ERICKSON, B.E., HELZ, G.R. (2000) Molybdenum(VI) speciation in sulfidic waters: Stability and lability of thiomolybdates. *Geochimica et Cosmochimica Acta* 64, 1149–1158.

HELZ, G.R., VORLICEK, T.P. (2019) Precipitation of molybdenum from euxinic waters and the role of organic matter. *Chemical Geology* 509, 178–193.

KENDALL, B., KOMIYA, T., LYONS, T.W., BATES, S.M., GORDON, G.W., ROMANIELLO, S.J., JIANG, G., CREASER, R.A., XIAO, S., McFADDEN, K., SAWAKI, Y. (2015) Uranium and molybdenum isotope evidence for an episode of widespread ocean oxygenation during the late Ediacaran Period. *Geochimica et Cosmochimica Acta* 156, 173–193.

KENDALL, B., DAHL, T.W., ANBAR, A.D. (2017) The stable isotope geochemistry of molybdenum. *Reviews in Mineralogy and Geochemistry* 82, 683–732.

KENDALL, B., WANG, J., ZHENG, W., ROMANIELLO, S.J., OVER, D.J., BENNETT, Y., XING, L., KUNERT, A., BOYES, C., LIU, J. (2020) Inverse correlation between the molybdenum and uranium isotope compositions of Upper Devonian black shales caused by changes in local depositional conditions rather than global ocean redox variations. *Geochimica et Cosmochimica Acta*, doi: 10.1016/j.gca.2020.01.026.

KERL, C.F., LOHMAYER, R., BURA-NAKIĆ, E., VANCE, D., PLANER-FRIEDRICH, B. (2017) Experimental confirmation of isotope fractionation in thiomolybdates using ion chromatography and detection by multi-collector ICP-MS. *Anaytical Chemistry* 89, 3123–3129.

LAU, K.V., LYONS, T.W., MAHER, K. (2020) Uranium reduction and isotopic fractionation in reducing sediments: Insights from reactive transport modelling. *Geochimica et Cosmochimica Acta*, doi: 10.1016/j.gca.2020.01.021.

NEUBERT, N., NÄGLER, T.F., BÖTTCHER, M.E. (2008) Sulfidity controls molybdenum isotope fractionation in euxinic sediments: evidence from the modern Black Sea. *Geology* 36, 775–778.

NÄGLER, T.F., ANBAR, A.D., ARCHER, C., GOLDBERG, T., GORDON, G.W., GREBER, N.D., SIEBERT, C., SOHRIN, Y., VANCE, D. (2014) Proposal for an international molybdenum isotope measurement standard and data representation. *Geostandards. Geoananalytical Research* 38, 149–151.

SCHUNCK, H., LAVIK, G., DESAI, D. K., GROSSKOPF, T., KALVELAGE, T., LOESCHER, C.R., PAULMIER A., CONTRERAS, S., SIEGEL, H., HOLTAPPELS, M., ROSENSTIEL, P., SCHILHABEL, M.B., GRACO, M., SCHMITZ, R.A., KUYPERS, M.M.M., LaROCHE, J. (2013) Giant hydrogen sulfide plume in the oxygen minimum zone off Peru supports chemolithoautotrophy. *PLoS ONE* 8, doi: 10.1371/journal.pone.0068661.

VADSARIA, T., RAMSTEIN, G., DUTAY, J.-C., LI, L., AYACHE, M., RICHON, C. (2019) Simulating the occurrence of the last sapropel event (S1): Mediterranean basin ocean dynamics simulations using Nd isotopic composition modeling. *Paleoceanography and Paleoclimatology* 34, 237–251, doi: 10.1029/2019PA003566.

Rapid onset of ocean anoxia shown by high U and low Mo isotope compositions of sapropel S1

M.B. Andersen, A. Matthews, M. Bar-Matthews, D. Vance

Supplementary Information

The Supplementary Information includes:

1. Methods

The samples from sapropel S1 were taken from ODP core 967D, drilled at a water depth of 2550m south of Cyprus, at the base of the northern slope of the Eratosthenes Seamount (Emeis *et al*., 1998) (Fig. S-1). This study uses the dried and sieved <63μm fraction of the samples analysed by Scrivner *et al*. (2004) and Vance *et al*. (2004) for Nd isotope measurements in foraminifera (ODP 967D-1H1, covering S1 and depths immediately above and below). The S5 data of Andersen *et al*. (2018) used in this study were also measured on the dried and sieved <63 μm fraction of the samples analysed by Scrivner *et al*. (2004) for Nd isotopes in foraminifera (ODP 967C-H5). Previous studies using the <63 μm fractions indicate that they provide a representative record of the elemental and isotope geochemistry of sapropels (Box *et al*., 2011; Azrieli-Tal *et al*., 2014). Sample preparation and U isotope measurements were conducted at the facilities of the Bristol Isotope Group, University of Bristol, United Kingdom, while chemical analyses of major and trace element chemical analyses (wt.% and μg/g, respectively) were made using Induction Coupled Optical Emission Spectroscopy (ICP-OES) and Inductively Coupled Plasma Mass Spectrometry (ICP-MS) at the Geological

Survey of Israel after low temperature ashing and sodium peroxide digestions. Errors on single values (1σ) are from ± 5 % and ± 7 % for ratios. Total organic carbon (TOC) data (for the bulk sediment) are taken from Vance *et al.* (2004). For samples missing a direct TOC measurement, the TOC is estimated as an average of the two bracketing samples with available TOC data.
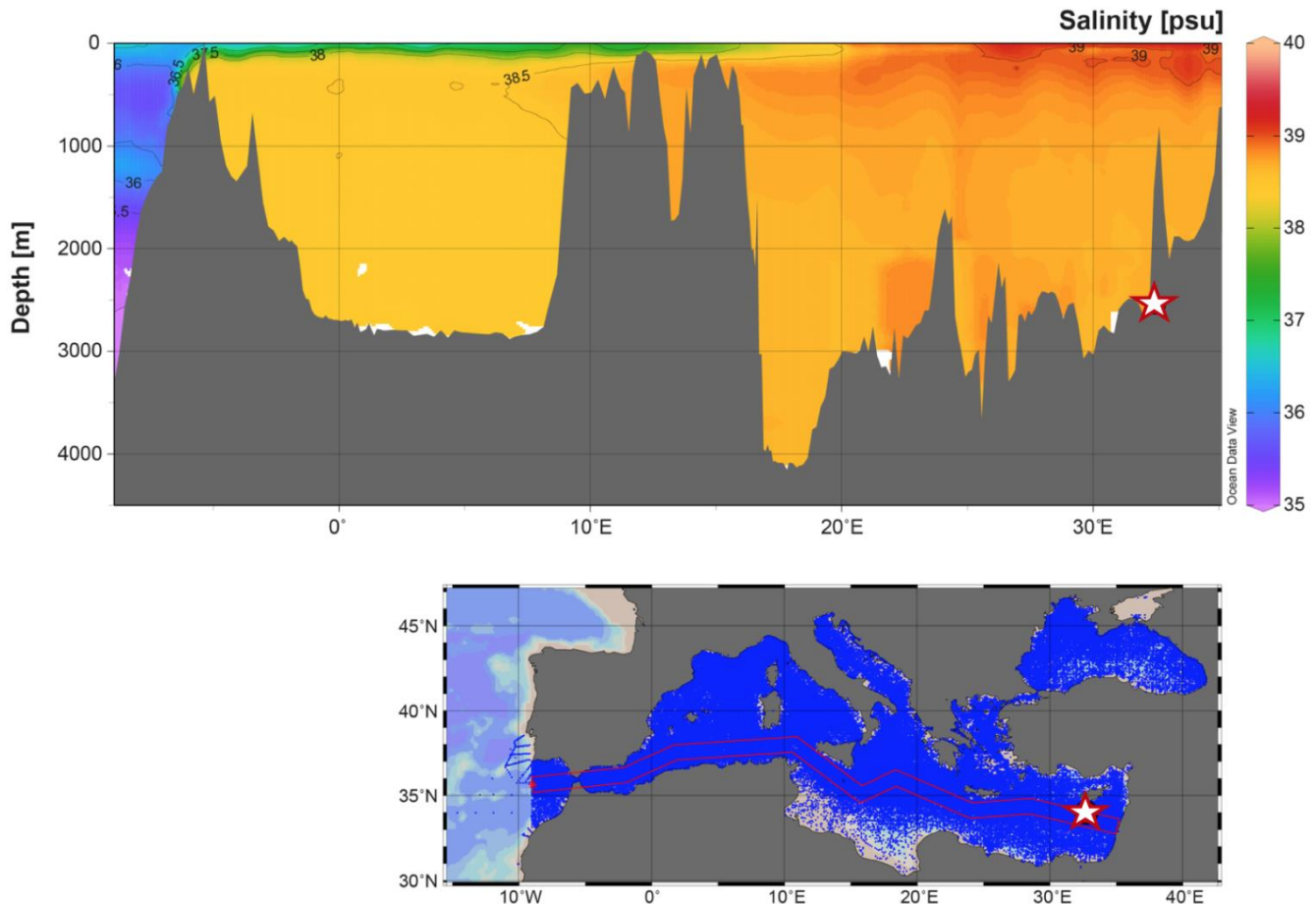
Figure S-1   Vertical salinity profile (top) through the present-day Mediterranean basin (bottom). The position of core ODP 967 (2550 m water depth) is marked (star). Present-day deep-waters are well oxygenated due to thermohaline circulation driven by surface water evaporation and high salinity in the EM. The periodic formation of organic carbon-rich sapropels correlated with high northern hemisphere summer insolation during minima in the *ca* 21 ka orbital precession cycle. Significantly slower deep-water renewal rates in the EM would have played an important role in the formation of sapropels and are consistent with the suppression of overturning during high insolation periods, due to increased water body stratification resulting from higher riverine freshwater input under enhanced monsoon forcing. Diagram generated in Ocean Data View (https://odv.awi.de).

Details of the molybdenum and uranium isotope analyses, including standards, calibration procedures, and error treatments, are given in Azrieli-Tal *et al.* (2014) and Andersen *et al.* (2018). In brief, for the uranium isotope work in this study, samples (10-50 mg) were dissolved in steps involving concentrated HNO_3, HF, HCl and H_2O_2. At the first dissolution step, in HNO_3 and HF, the IRMM3636 $^{236}U/^{233}U$ double spike was added, aiming for a $^{236}U/^{235}U$ of ~4. After heating, fluxing and subsequent drying steps using 6 M HCl (x2) and a 7 M HNO_3 + 30% H_2O_2 mixture were completed, samples were re-dissolved in 10 ml of 3 M HNO_3 in preparation for U-Teva chromatographic chemistry, following protocols given in Andersen *et al.* (2014; 2018). Purified U fractions were dried and prepared for mass spectrometry in 2% (v/v) HCl aiming for 100-200 ppb U. Full procedural chemistry blanks were <20 pg of U. Uranium isotopic analyses were carried out at the University of Bristol, using a ThermoQuest Neptune instrument operating at low mass resolution (M/ΔM

~500) by means of a CPI (Amsterdam, The Netherlands) PFA nebulizer and spray chamber fitted to a CETAC Aridus. The set-up and measurement protocols were as outlined in Andersen *et al.* (2014; 2015). All Faraday cups were equipped with $10^{11}\,\Omega$ resistors, apart from the cup for ^{238}U ($10^{10}\,\Omega$). Measurements were conducted with "standard" sampler and "X" type skimmer cones. Typical sample ion beam intensities were ~1 nA for ^{238}U using ~50 ng U per analysis. Measurements of two unknowns were bracketed with the CRM-145 uranium standard, spiked in similar fashion as the unknowns. The in-house CZ-1 uraninite standard, processed through U-Teva chemistry and periodically measured in a similar fashion to the sediment samples, yielded δ^{238}U of – 0.055±0.032 (±2S.D.) for ten repeats, in excellent agreement with previously published compositions for this standard (Stirling *et al.*, 2007; Andersen *et al.*, 2015). The ^{234}U/^{238}U ratios were measured simultaneously with the ^{235}U/^{238}U, and the ^{234}U/^{238}U data are reported as δ^{234}U, the ^{234}U/^{238}U relative to secular equilibrium in part per thousand using the half-lives of Cheng *et al.* (2013). The external reproducibility for the CZ-1 standard is used as the uncertainty estimate for each of the unknowns (Andersen *et al.*, 2014; 2015; 2018). Sample data, including depth information, chemical element concentrations, and isotopic compositions used in this study are presented in Table S-1.

2. Age Model and Sapropel Event Definitions

The age model for S1 (10.8 to 6.1 ka) is taken from de Lange *et al.* (2008) and from Grant *et al.* (2012) for S5 (128.3 to 121.5 ka). The upper and lower boundaries assigned to the sapropels S1 and S5 are determined from their Ba/Al and TOC profiles (130-106 cm and 103.5- 74 cm, respectively; Azrieli-Tal *et al.*, 2014; Andersen *et al.*, 2018, see Figure S-2). Whereas the TOC and Ba/Al boundaries coincide in S5, the TOC profile in S1 indicates post-sapropel oxidation (burndown) in its upper 4 cm (106-110 cm) (Fig. S-2). Sapropel geochemical data for S1 *sensu stricto* are thus recorded from ~110 to 130 cm. Furthermore, a short-lived oxidation event commencing at ~116 cm is also evident from the molybdenum isotope, Fe/Al and Ba/Al data (Azrieli- Tal *et al.*, 2014). This likely correlates with a re-ventilation event related to the 8 ka northern hemisphere cold climate event recorded in other EM S1 sapropels (Casford *et al.,* 2003). This injection of oxygen by re-ventilation has been recognised in number of sapropel S1 samples and is shown to affect (in addition to Ba/Al) redox sensitive metal ratios such as Fe/Al, As/Al and V/Al (Hennekam *et al.*, 2014 ; Tachikawa *et al.*, 2015 ; Filippidi and de Lange, 2019). The preservation in ODP967 of this re-ventilation signal (which has lead researchers to classify S1 into early (S1a) and late (S1b) segments) is not consistent with post-sapropel diagenetic remobilization of reduction sensitive metals from upper S1b into lower S1a. Specifically for U, a re-distribution profile would be expected to show increasing U/Al from the top and down to a zone of maximum reduction within S1a, similar to observed in modern reducing sediments with increasing uptake of reduced U at depth (*e.g.,* Abshire *et al.*, 2020). The lack of such U (Fig. 1) or U/Al (Fig. S-2) profile, combined with the TOC and Ba/Al profiles for S1 and S5, is compatible with the early/late peak sapropel development evident in redox sensitive elements (Fig. S-2). This is also true for EM S1 and S5 TOC, Ba/Al and redox metal sapropel profiles determined in other studies (*e.g.,* Gallego-Torres *et al.*, 2007; 2010).
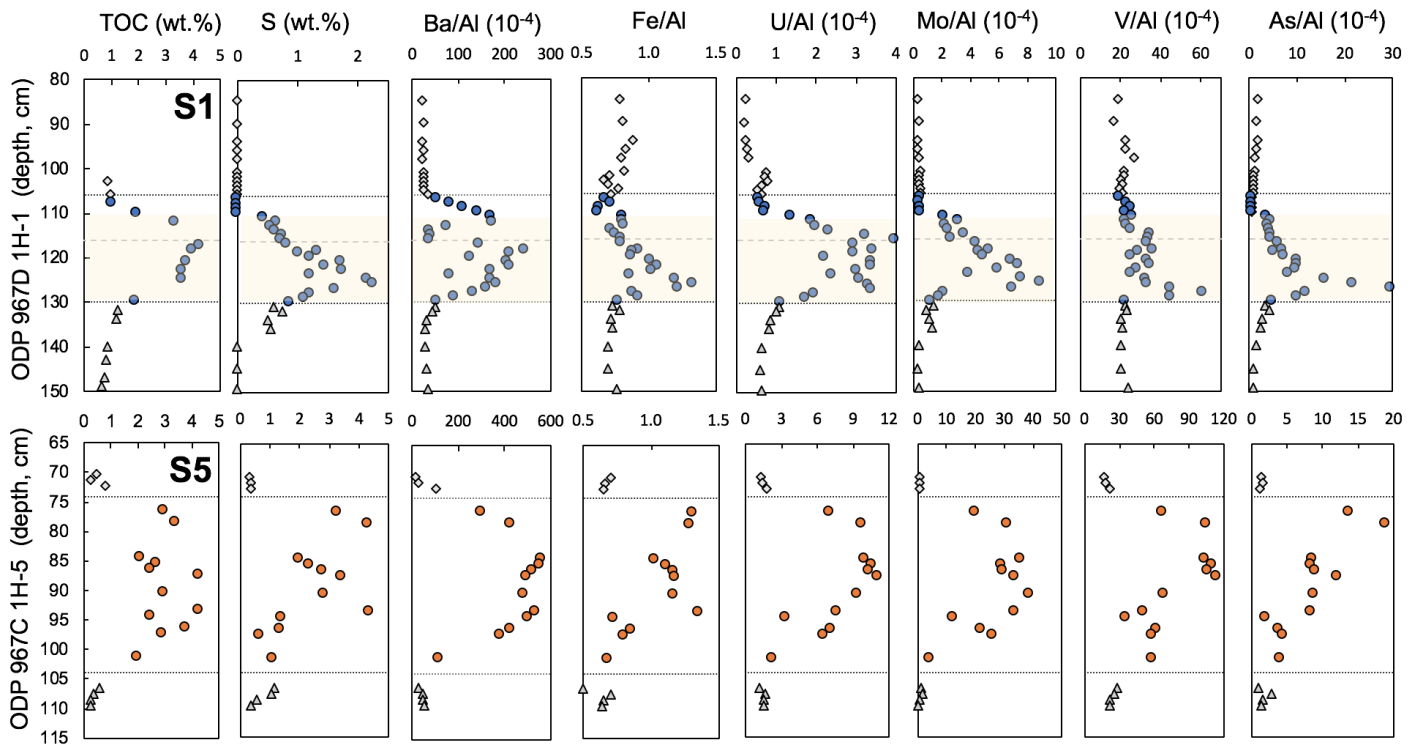
Figure S-2 Depth profiles of selected proxies (TOC, S, Ba/Al, Fe/Al, U/Al, Mo/Al, V/Al, As/Al) for sapropel S1 (top layer) and sapropel S5 (lower layer). (Data sources for this figure and main text Figure 1, S1: Azrieli-Tal *et al.*, 2014; Vance *et al.*, 2004; this study; S5: Andersen *et al.*, 2018; Emeis *et al.*, 1998 –see Table S-1). Stippled lines represent sapropel boundaries. The additional dashed line at 116 cm in S1 represents the commencement of the 8 ka reventilation event, and the yellow shading defines the unaltered sapropel below the depth to which the effects of the post-sapropel burndown were felt. The data clearly show the different timing of the peak increase in redox sensitive proxies early in S1 *vs*. late in S5. Note the different scales between S1 and S5 for a range of elemental and ratios (S, Ba/Al, U/Al, Mo/Al, V/Al, As/Al).

3. *Organic Carbon Sediment Accumulation Rates*

Organic carbon accumulation rates (OCAR) at peak sapropel conditions were calculated using the equation OCAR = 1000 * TOC * ρ * LSR mg/cm^2.ky (Gallego-Torres *et al.*, 2007; Algeo *et al.*, 2013; Schoepfer *et al.*, 2015), where ρ is the dry sediment density and TOC is the mean TOC wt. fraction (g/g). Mean TOC fraction (Fig. S-2) and standard deviation (1SD) data are 0.0382 ± 0.0028 for peak S1 data (126-118 cm) and 0.0316 ± 0.0.77 for peak S5 data (94-76 cm). S1 and S5 have similar thicknesses at ODP 967 (24 *vs* 29.5 cm), but the longer duration of S5 (6.8 *vs*. 4.7 ky) means that it has a slightly lower linear sedimentation rate (LSR) of 4.3 cm/ky compared to 5.1 cm/ky for S1). The ρ values are taken from S1 and S5 data at EM ODP site 964 (1.34 ±0.08 and 1.31 ± 0.03 g/cm^3, respectively (Gallego-Torres *et al.*, 2007)). Calculated OCAR values at ODP 967 are: 261 ± 36 mg/cm^2.ky (S1): 178 ± 48 mg/cm^2.ky (S5). These values are comparable with average OCAR values calculated for the Black Sea (Schoepfer *et al.*, 2015) and emphasise the fact that peak S1 has a high organic carbon flux, despite apparently lower deep-water sulfide levels than S5.

4. Authigenic U and Mo Concentration and Isotope Estimates

Authigenic U (U_{auth}) and molybdenum (Mo_{auth}) were calculated from the U and Mo enrichment factors relative to Post Archaean Average Shale (PAAS; Taylor & McLennan, 1985) U/Al and Mo/Al ratios, which are taken to represent the detrital component (Thomson *et al.*, 1999; Brumsack, 2006; Tribovillard *et al.*, 2006). Such a calculation (Table S-1) shows that the detrital fraction (U_{det}) is a significant component of the background sediments: overlying post-sapropel sediments U_{det} ~ 50% falling to < 20% within 5 cm of the boundary: Mo_{det} ~ 50% falling to ~ 30%; underlying pre-sapropel sediments U_{det} ~ 19-11%; Mo_{det} ~ 46-15%. U_{auth} and Mo_{auth} fractions in S1 vary from 85% to 99%, with values >96% typical of peak sapropel conditions.

These detrital U estimates are consistent with the measured $\delta^{234}U$ (Table S-1). The Holocene age of the samples means that the age correction for the $\delta^{234}U$ is less than a few permil and the sapropels are likely to have experienced minimal ^{234}U nuclide redistribution, as has been observed in other sapropels (Gourgiotis *et al.*, 2011), and is also likely the case for the S5 samples (Table S-1). The $\delta^{234}U$ values are high for S1 (~130-115‰), slightly lower for pre-S1 (~110-100‰) and lowest for post-S1 (~90-0‰) sediments. While modern seawater has a $\delta^{234}U$ of ~146‰, the detrital material can be variable and deviate from secular equilibrium. It is therefore not possible to accurately estimate the authigenic U fraction in the absence of good estimates of the detrital terrigenous $\delta^{234}U$ composition. We note however that the $\delta^{234}U$ compositions from highest to lowest values of S1, followed by pre-S1 and then post-S1, are in good agreement with the order of high to low authigenic U based on U/Al.

The isotope composition of the authigenic Mo and U fractions is estimated using the elemental concentrations in combination with Mo and U isotope compositions for detrital terrigenous shales. Here, values of $\delta^{238}U$ = -0.3‰ and $\delta^{98}Mo$ = 0‰ were used for the detrital terrigenous sediments (Tissot & Dauphas, 2015; Andersen *et al.*, 2017; Kendall *et al.*, 2017; Andersen *et al.*, 2018). Propagation of uncertainties on the authigenic composition was done by weighting the relative size of the detrital component following Andersen *et al.*, (2014) and (2018), see Table S-1. Furthermore, authigenic $\delta^{238}U$ and $\delta^{98}Mo$ from literature data (Asael *et al.*, 2013 ; Kendall *et al.*, 2015; Cheng *et al.*, 2020; Kendall *et al.*, 2020) was reconverted in similar fashion to the sapropel data (apart from omitting the 'carbonate' correction for the authigenic U, see below) and using Mo-U isotope and Mo-U *vs*. Al ratios reported in these publications (Table S-1).

5. Authigenic $\delta^{238}U$ and $\delta^{98}Mo$ - Estimating the Contribution from U and Mo Directly Associated with Organic Matter

Andersen *et al.* (2014) suggested that authigenic U was dominated by two main fractions, (i) U from biogenic carbonates and (ii) U incorporated from *in situ* uranium reduction. Following calculations in Andersen *et al.* (2014), which assume that the [Ca] in bulk sediments is primarily from biogenic carbonates with ~1 ppm U, the relative U contribution from this carbonate source to the authigenic fraction can be estimated. This calculation shows that the biogenic carbonate U fraction constitutes <3% for S1 and <20% for surrounding sediments (Table S-1). Further, the $\delta^{238}U$ of the remaining authigenic U fraction may be estimated by subtracting the biogenic U carbonate fraction with $\delta^{238}U$ = -0.4‰ (Andersen *et al.*, 2014). These calculations suggest that the greater part of U_{auth} in these sediments is due to authigenic U addition rather than that associated with biogenic carbonates. In addition to U uptake from *in situ* U reduction (process ii), it has also been suggested that U may be directly associated with organic matter (OM) which could be a third (iii) potential important additional source of authigenic U accumulation in sediments. This OM-derived U, either directly incorporated or adsorbed, could carry isotopically light U to the sediments (Holmden *et al.*, 2015; Hinojosa *et al.*, 2016; Andersen *et al.*, 2017; Abshire *et al.*, 2020; Chen *et al.*, 2020). Such a U fraction would

be indistinguishable from the *in situ* uranium reduction component (process ii) in the calculations described above, and may drive the authigenic $\delta^{238}U$ pool towards lower compositions, in instances when the relative OM deposition rate *vs.* *in situ* reduction rate is high.

Focusing on the pre-S1 and early part of the S1 data with relatively low [U_{auth}] in the sediments, $1/[U_{auth}]$ *vs.* $\delta^{238}U$ plots (Fig S-3a) show a systematic evolution from low $\delta^{238}U_{auth}$ (~ -0.6‰) at low [U_{auth}], to high $\delta^{238}U_{auth}$ (~ +0.5‰) at high [U_{auth}]. This pattern is consistent with an approximate mixing trend between authigenic OM-derived U ($\delta^{238}U$ ~ -0.6) and increasingly *in situ* U reduction. The $1/[U_{auth}]$ *vs.* $\delta^{238}U$ plots for the S1 and S5 and background sediment data (Fig S-3b) show that the post-S1 data also plot in the region that may be dominated by authigenic OM-derived U, but with significantly lower [U_{auth}]. Also, both the post- and pre-S5 data show moderate U enrichments, which could suggest a mixture between authigenic OM-derived U and *in situ* U reduction. On the other hand, Andersen *et al.* (2018) interpreted these samples to show U and Mo isotope systematics consistent with near quantitative uptake of U and Mo from porewaters. Both scenarios are possible. In contrast, both peak S1 and peak S5 appear to be completely dominated by authigenic *in situ* U reduction uptake, but with differently expressed U isotope fractionations as discussed in the main text.
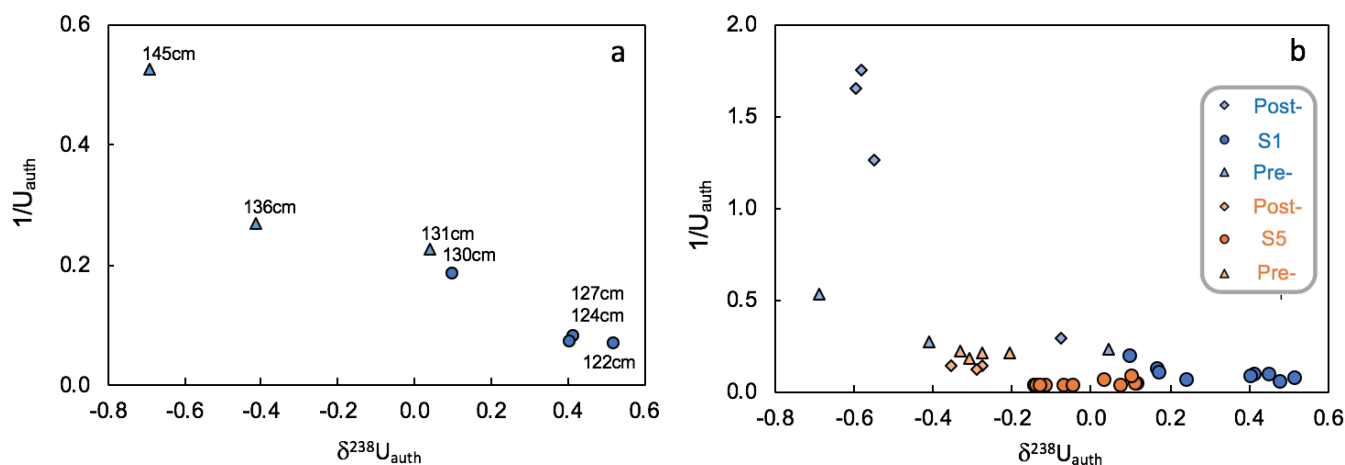
Figure S-3   **(a)** Cross-plots of $\delta^{238}U$ vs. $1/U_{auth}$ (ppm^{-1}) from pre-S1 and the early part of S1 (from 145 to 120 cm depth) and **(b)** all the data from S1/S5 and surrounding sediments. The $\delta^{238}U$ vs. $1/U_{auth}$ plot in (a) suggests that the data define a possible mixing trend between authigenic U associated with organic matter ($\delta^{238}U$ ~ -0.6‰ and low U_{auth}) and U formed by in situ reduction ($\delta^{238}U$ ~ +0.5‰ and high U_{auth}) at peak sapropel conditions.

Similar to the above discussion of the authigenic U uptake, although Mo associated with biogenic carbonate is low and therefore not important for authigenic calculations, the potential for OM-derived Mo has been suggested as a potential important source for Mo addition to organic carbon-rich sediments (e.g. McManus *et al.*, 2002; King *et al.*, 2018). Based on cross-plots of $\delta^{98}Mo$ *vs.* $1/[Mo_{auth}]$ for the S1 and S5 and surrounding data (Fig. S-4) there are no trends evident in the data which could suggest that this is an important process for the observed $\delta^{98}Mo_{auth}$ in the organic carbon-rich sapropel sediments. There is, however, a difference in the $\delta^{98}Mo_{auth}$ compositions of the background sediments. The background sediments surrounding S1 have $\delta^{98}Mo_{auth}$ values in the range of suboxic sediments with low sulfide levels, where Mo uptake could be dominated by OM or adsorption on Fe oxides (*e.g.,* McManus *et al.*, 2002; Goldberg *et al.*, 2009; Scholz *et al.*, 2013; Matthews *et al.*, 2017). On the other hand, S5 background sediments have $\delta^{98}Mo_{auth}$ values >+1.5‰, typical of sediments where authigenic Mo uptake occurs within sulfidic pore waters (Poulson-Brucker *et al.*, 2009; 2012).
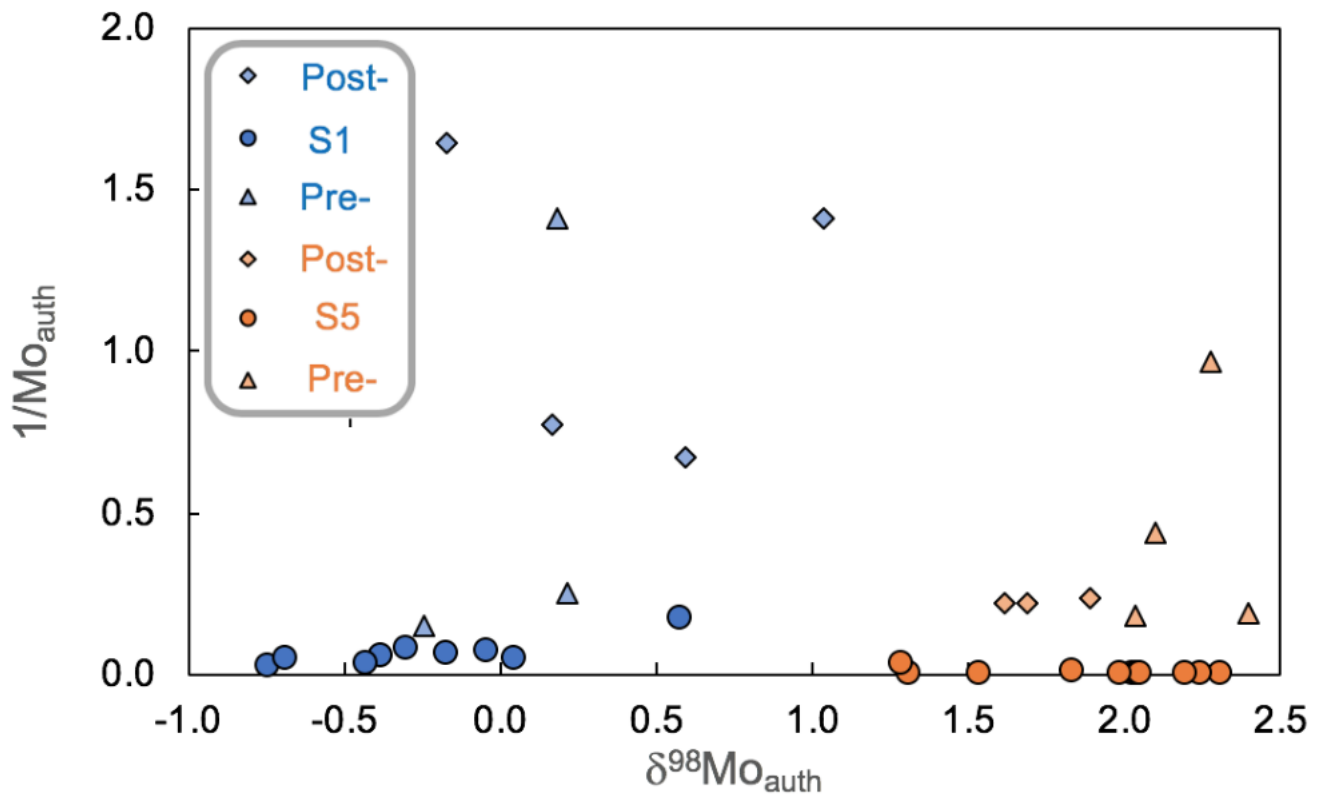
Figure S-4 $\delta^{98}Mo$ vs. $1/Mo_{auth}$ (ppm^{-1}) cross-plot for S1 and S5 and non-sapropel sediment data. No clear mixing trends are observed between post/pre-S1 or S5 and the peak S1 and S5 sediments.

Supplementary Tables

Table S-1 is available for download (Excel file) at http://www.geochemicalperspectivesletters.org/article2027.

Table S-1   **(a)** Sapropel S1 and S5, U and Mo isotope data and concentration data, incl. authigenic estimates. **(b)** Extended trace metal concentration data for sapropel S1. **(c)** Authigenic U and Mo isotope calculations for literature data.

Supplementary Information References

Abshire, M.L., Romaniello, S.J., Kuzminov, A.M., Cofrancesco, J., Severmann, S., Riedinger, N. (2020) Uranium isotopes as a proxy for primary depositional redox conditions in organic-rich marine systems. *Earth and Planetary Science Letters* 529, 115878.

Algeo, T.J., Henderson, C.M., Tong, J., Feng, Q., Yin, H., Tyson, R.V. (2013) Plankton and productivity during the Permian–Triassic boundary crisis: An analysis of organic carbon fluxes. *Global and Planetary Change* 105, 52-67.

Andersen, M.B. Romaniello, S., Vance, D., Little, S.H., Herdman, R., Lyons, T.W. (2014) A modern framework for the interpretation of 238U/235U in studies of ancient ocean redox. *Earth and Planetary Science Letters* 400, 184-194.

Andersen, M.B., Elliott, T., Freymuth, H., Sims, K.W., Niu, Y., Kelley, K.A. (2015) The terrestrial uranium isotope cycle. *Nature* 517, 356-359.

Andersen, M.B., Stirling, C.H., Weyer, S. (2017) Uranium isotope fractionation. *Reviews in Mineralogy and Geochemistry* 82, 799-850.

Andersen, M.B., Matthews, A., Vance, D., Bar-Matthews, M., Archer, C., de Souza, G.F. (2018) A 10-fold decline in the deep Eastern Mediterranean thermohaline overturning circulation during the last interglacial period. *Earth and Planetary Science Letters* 503, 58-67.

Asael D, Tissot FL, Reinhard CT, Rouxel O, Dauphas N, Lyons TW, Ponzevera E, Liorzou C, Chéron S. (2013) Coupled molybdenum, iron and uranium stable isotopes as oceanic paleoredox proxies during the Paleoproterozoic Shunga Event. *Chemical Geology* 362,193–210.

Azrieli-Tal, I., Matthews, A., Bar-Matthews, M., Almogi-Labin, A., Vance, D., Archer, C., Teutsch, N. (2014) Evidence from molybdenum and iron isotopes and molybdenum–uranium covariation for sulphidic bottom waters during Eastern Mediterranean sapropel S1 formation. *Earth and Planetary Science Letters* 393, 231-242.

Box, M.R., Krom, M.D., Cliff, R.A., Bar-Matthews, M., Almogi-Labin, A., Ayalon, A., Paterne, M. (2011) Response of the Nile and its catchment to millennial-scale climatic change since the LGM from Sr isotopes and major elements of East Mediterranean sediments. *Quaternary Science Reviews* 30, 431-442.

Brumsack, H.-J. (2006) The trace metal content of recent organic carbon-rich sediments: Implications for Cretaceous black shale formation, *Palaeogeography, Palaeoclimatology, Palaeoecol*ogy, 232, 344-361.

Casford, J. S. L., Rohling, E. J., Abu-Zied, R. H., Fontanier, C., Jorissen, F. J., Leng, M. J., Schmiedl, G., Thomson, J. (2003) A dynamic concept for eastern Mediterranean circulation and oxygenation during sapropel formation. *Palaeogeography, Palaeoclimatology, Palaeoecology* 190, 103–119.

Chen, X., Zheng, W., Anbar, A.D. (2020) Uranium Isotope Fractionation (238U/235U) during U (VI) Uptake by Freshwater Plankton. *Environmental Science & Technology* 54, 2744-2752.

Cheng, H., Edwards, R.L., Sehe, C.C ., Polyak, V.J., Asmerom, Y., Woodhead, Y., Hellstrom, J., Wang, Y., Kong, X., Spötl, C., Wang, X. and Alexander Jr., C. (2013) Improvements in ²³⁰Th dating, ²³⁰Th and ²³⁴U half-life values, and U-Th isotopic measurements by multi-collector inductively couples plasma mass spectrometry. *Earth and Planetary Science Letters* 371-372, 82-91.

Cheng, M., Li, C., Jin, C., Wang, H., Algeo, T.J., Lyons, T.W., Zhang, F. and Anbar, A. (2020) Evidence for high organic carbon export to the early Cambrian seafloor. *Geochimica et Cosmochimica Acta, doi:* 10.1016/j.gca.2020.01.050.

de Lange, G.J., Thomson, J., Reitz, A., Slomp, C.P., Speranza Principato, M., Erba, E., Corselli, C. (2008) Synchronous basin-wide formation and redox-controlled preservation of a Mediterranean sapropel. *Nature Geoscience* 1, 606–610.

Emeis, K.C., Schulz, H.M., Struck, U., Sakamoto, T., Doose, H., Erlenkeuser, H., Howell, M., Kroon, D., Paterne, M. (1998) Stable isotope and alkenone temperature records of sapropels from sites 964 and 967: constraining the physical environment of sapropel formation in the eastern Mediterranean sea. In: Robertson, A.H.F., Emeis, K.C., Richter, C., Camerlenghi, A. (Eds.) *Proceedings of the Ocean Drilling Program, Scientific Results* 160, 309-331.

Filippidi, A. & de Lange G.J. (2019) Eastern Mediterranean deep water formation during sapropel S1: a reconstruction using geochemical records along a bathymetric transect in the Adriatic outflow region. *Paleoceanography and Paleoclimatology*, 34, 409–429. doi: 10.1029/2018PA003459.

Gallego-Torres, D., Martínez-Ruiz, F., Paytan, A., Jiménez-Espejo, F.J., Ortega-Huertas, M. (2007) Pliocene–Holocene evolution of depositional conditions in the eastern Mediterranean: role of anoxia vs. productivity at time of sapropel deposition. *Palaeogeography, Palaeoclimatology, Palaeoecology* 246, 424–439.

Gallego-Torres, D., Martinez-Ruiz, F., de Lange, G. J., Jimenez-Espejo, F.J. Ortega-Huertas, M. (2010) Trace-elemental derived paleoceanographic and paleoclimatic conditions for Pleistocene Eastern Mediterranean sapropels. *Palaeogeography, Palaeoclimatology, Palaeoecology* 293, 76–89.

Goldberg, T., Archer, C., Vance, D., Poulton, S.W. (2009) Mo isotope fractionation during adsorption to Fe (oxyhydr)oxides. *Geochimica Cosmochimica Acta* 73, 6502–6516.

Gourgiotis A., Reyss, J.L., Frank, N., Guihou, A., Anagnostou, C. (2011) Uranium and radium diffusion in organic-rich sediments (sapropels). *Geochemistry, Geophysics, Geosystems* 12, Q09012.

Grant, K.M., Rohling, E.J., Bar-Matthews, M., Ayalon, A., Medina-Elizalde, M., Ramsey, C.B., Satow, C., Roberts, A.P. (2012) Rapid coupling between ice volume and polar temperature over the past 150,000 years. *Nature* 491, 744-747.

Hennekam, R., Jilbert, T., Schnetger, B., de Lange, G.J. (2014) Solar forcing of Nile discharge and sapropel S1 formation in the early to middle Holocene eastern Mediterranean. *Paleoceanography* 29, 2013PA002553, doi:10.1002/2013PA002553.

Hinojosa, J.L., Stirling, C.H., Reid, M.R., Moy, C.M., Wilson, G.S. (2016) Trace metal cycling and $^{238}U/^{235}U$ in New Zealand's fjords: Implications for reconstructing global paleoredox conditions in organic-rich sediments. *Geochimica et Cosmochimica Acta* 179, 89-109.

Holmden, C., Amini, M., Francois, R. (2015) Uranium isotope fractionation in Saanich Inlet: A modern analog study of a paleoredox tracer. *Geochimica et Cosmochimica Acta* 153, 202-215.

Kendall, B., Komiya, T., Lyons, T.W., Bates, S.M., Gordon, G.W., Romaniello, S.J., Jiang, G., Creaser, R.A., Xiao, S., McFadden, K., Sawaki, Y. (2015) Uranium and molybdenum isotope evidence for an episode of widespread ocean oxygenation during the late Ediacaran Period. *Geochimica et Cosmochimica Acta* 156, 173-193.

Kendall, B., Dahl, T.W., Anbar, A.D. (2017) The stable isotope geochemistry of molybdenum. *Reviews in Mineralogy and Geochemistry* 82, 683-732.

Kendall, B., Wang, J., Zheng, W., Romaniello, S.J., Over, D.J., Bennett, Y., Xing, L., Kunert, A., Boyes, C., Liu, J. (2020) Inverse correlation between the molybdenum and uranium isotope compositions of Upper Devonian black shales caused by changes in local depositional conditions rather than global ocean redox variations. *Geochimica et Cosmochimica Acta*, doi: 10.1016/j.gca.2020.01.026

King, E.K., Perakis, S.S., Pett-Ridge, J.C. (2018) Molybdenum isotope fractionation during adsorption to organic matter. *Geochimica et Cosmochim. Acta* 222, 584-598.

Matthews, A., Azrieli-Tal, I., Benkovitz, A., Bar-Matthews, M., Vance, D., Poulton, S.W., Teutsch, N., Almogi-Labin, A., Archer, C. (2017) Anoxic development of sapropel S1 in the Nile Fan inferred from redox sensitive proxies, Fe speciation, Fe and Mo isotopes. *Chemical Geology* 475, 24-39.

McManus, J., Nägler, T.F., Siebert, C., Wheat, C.G., Hammond, D.E. (2002) Oceanic molybdenum isotope fractionation: Diagenesis and hydrothermal ridge-flank alteration. *Geochemistry, Geophysics, Geosystems* 3, 1-9.

Poulson-Brucker, R.L., McManus, J., Severmann, S., Berelson, W.M. (2009) Molybdenum behavior during early diagenesis: insights from Mo isotopes. *Geochemistry, Geophysics, Geosystems* 10, doi: 10.1029/2008GC002180.

Poulson-Brucker, R.L., McManus, J., Poulton, S.W. (2012) Molybdenum isotope fractionation observed under anoxic experimental conditions. *Geochemical Journal* 46, 201-209.

Schoepfer, S.D., Shen, J., Wei, H., Tyson, R.V., Ingall, E., Algeo, T.J. (2015) Total organic carbon, organic phosphorus, and biogenic barium fluxes as proxies for paleomarine productivity. *Earth-Sciences Reviews* 149, 23-52.

Scholz, F., McManus, J., Sommer, S. (2013) The manganese and iron shuttle in a modern euxinic basin and implications for molybdenum cycling at euxinic ocean margins. *Chemical Geology* 355, 56–68

Scrivner, A., Vance, D., Rohling, E.J. (2004) New neodymium isotope data quantify Nile involvement in Mediterranean anoxic episodes. *Geology* 32, 565–568.

Stirling, C.H., Andersen, M.B., Potter, E.K., Halliday, A.N. (2007) Low temperature isotopic fractionation of uranium. *Earth and Planetary Science Letters* 264, 208-225.

Tachikawa, K., Vidal, L.-A., Cornuault, M., Garcia, M., Pothin, A., Sonzogni, C., Bard, E., Menot, G., Revel, M. (2015) Eastern Mediterranean Sea circulation inferred from the conditions of S1 sapropel deposition. *Climate of the Past* 11, 855–867.

Taylor R.N., McLennan, S. (1985) *The Continental Crust: Its Composition and Evolution.* Blackwell, Boston.

Thomson, J., Mercone, D., de Lange, G.J., van Santvoort, P.J.M. (1999) Review of recent advances in the interpretation of Eastern Mediterranean sapropel S1 from geochemical evidence. *Marine Geology* 153, 77–89.

Tissot, F.L.H., Dauphas, N. (2015) Uranium isotopic compositions of the crust and ocean: age corrections, U budget and global extent of modern anoxia. *Geochimica et Cosmochimica Acta* 167,113-143.

Tribovillard, N., Algeo, T.J., Lyons, T., Riboulleau, A. (2006) Trace metals as paleoredox and paleoproductivity proxies: An update. *Chemical Geology* 232, 12-32.

Vance, D., Scrivner, A.E., Beney, P, Staubwasser, M, Henderson, G.F., Stowell, N.C. (2004) The use of foraminifera as a record of past neodymium isotope composition of seawater. *Paleoceanography* 19, PA2009. doi:10.1029/2003PA000957